Comparison of Propagation Channel Characteristics for Multiple Millimeter Wave Bands

Jie Huang[1], Rui Feng[1], Jian Sun[1,2], Cheng-Xiang Wang[1,3], Wensheng Zhang[1], and Yang Yang[4]
[1]Shandong Provincial Key Lab of Wireless Communication Technologies, Shandong University, Jinan, 250100, China.
[2]State Key Lab. of Millimeter Waves, Southeast University, Nanjing, 210096, China.
[3]Institute of Sensors, Signals and Systems, School of Engineering & Physical Sciences, Heriot-Watt University, Edinburgh, EH14 4AS, UK.
[4]Shanghai Research Center for Wireless Communications (WiCO), Shanghai, 201210, China.
Email: hj_1204@sina.cn, fengxiurui604@163.com, sunjian@sdu.edu.cn, cheng-xiang.wang@hw.ac.uk, zhangwsh@sdu.edu.cn, yang.yang@wico.sh

***Abstract*—Millimeter wave (mmWave) communication has been a key technology for the fifth generation (5G) wireless communications. There have been various mmWave channel measurements. However, many measurements in the literature are conducted with different configurations, which may have large impacts on the propagation channel characteristics, and make the comparison of propagation channel characteristics for different mmWave bands impossible. In this paper, we carry out channel measurements at 11, 16, 28, and 38 GHz bands in an indoor environment using a vector network analyzer (VNA). The space-alternating generalized expectation-maximization (SAGE) algorithm is used to obtain the multipath component (MPC) parameters including three dimensional (3D) angular domain information. The propagation characteristics like average power delay profile (APDP), power azimuth profile (PAP), power elevation profile (PEP), root mean square (RMS) delay spread (DS), and azimuth and elevation angular spread (AS) are shown and compared for the four frequency bands. The results show similar properties for different bands and indicate the possibility of the derivation of a unified channel model framework for 10–40 GHz bands.**

***Index Terms*—Millimeter wave, 5G, SAGE, parameter estimation.**

I. Introduction

MmWave communication has been considered as a key technology for the 5G wireless communications [1], e.g., for wideband cellular communication (hotspot and small cell), wireless backhaul, indoor and device-to-device (D2D) communications [2]. MmWave generally corresponds to the 30–300 GHz bands, but sometimes the 10–30 GHz bands are also included as they share some similar propagation characteristics. Compared to the traditional sub 6 GHz frequency bands, mmWave has larger available bandwidth but suffers from additional higher path loss. Recently, many groups and standards including METIS [3], MIWEBA [4], mmMAGIC [5], 5GCM [6], 3GPP 38.900 [7], and NYU Wireless [8] have tried to develop mmWave channel models for the frequency range from 6 GHz to 100 GHz.

Various channel measurements have been conducted at some popular mmWave frequency bands, such as 11, 15, 28, 38, 60, and 73 GHz bands. In [9], 11 GHz outdoor urban cellular channel measurements were conducted using a 24×24 multiple-input multiple-output (MIMO) channel sounder with 400 MHz signal bandwidth and dual-polarized 12-element uniform circular arrays. Path loss, shadowing, cell coverage, polarization properties, and RMS DS were obtained. In [10], 15 GHz channel measurements were conducted using a VNA and a spectrum analyzer with 1 GHz bandwidth in two indoor corridor environments. Parameters like large-scale fading, Ricean K-factor, and RMS DS were obtained, as well as their statistical properties. In [11], a sliding correlator based direction-scan-sounding method was used to measure the 28 GHz indoor office environment with 500 MHz bandwidth. Both line-of-sight (LOS) and non-line-of-sight (NLOS) scenarios were considered, and the SAGE algorithm was applied to estimate delay and angular parameters of MPCs. In [12], the authors conducted 28 GHz measurements in an urban environment with 250 MHz bandwidth. The transmitter (Tx) antenna was scanned in both azimuth and elevation angle domains. After post-processing the angular power delay profiles (PDPs) and omni-directional measurements were synthesized. In [13], a commercial backhaul equipment was used to conduct channel measurements at 38 GHz in urban outdoor and outdoor-to-indoor environments. The LOS propagation, reflection, scattering, diffraction, transmission, as well as polarization effects were studied. Authors in [14] measured the 60 GHz channel with 4 GHz bandwidth in indoor conference room and office environments. At both ends of Tx and receiver (Rx), virtual planar array was utilized to investigate the influence of array size on beamforming performance. Prof. T. S. Rappaport et al. from New York University had also conducted various channel measurements at 28, 38, 60, and 73 GHz bands in campus, base station-mobile access, peer-to-peer, and vehicular scenarios [15]–[17].

However, most of the measurements in the literature were conducted with different channel sounders, measurement environments, antenna configurations, and even post-processing methods, which may have large impacts on the propagation channel characteristics, and make the comparison of propagation channel characteristics for different mmWave bands impossible. Thus it is unable to have a fair comparison of the available mmWave channel measurement results, though the comparison is very important for the development of a unified channel model framework for the whole mmWave bands.

To fill this gap, we carry out channel measurements at

978-1-5090-5932-4/17/$31.00 ©2017 IEEE

four frequency bands centered at 11, 16, 28, and 38 GHz in an indoor office environment using a VNA. The SAGE algorithm is applied to process the measurement data. The spatial-temporal propagation characteristics like APDP, PAP, PEP, RMS DS, and azimuth and elevation AS for the four frequency bands are extracted and compared.

The remainder of this paper is organized as follows. Section II describes the measurement environment and measurement system setup. In Section III, the SAGE algorithm and propagation channel characteristics are presented. The propagation channel characteristics comparison and analysis are described in Section IV. Finally, conclusions are drawn in Section V.

II. MmWave Channel Measurements

A. Measurement Environment

The channel measurements are conducted in an indoor office environment with room size of $7.2\times7.2\times3$ m^3, as shown in Fig. 1(a) [18]. The office is furnished with multiple chairs, desks, and a table. In addition, the desks and table are equipped with several computers and electronic devices. Other large objects include a closet, an air conditioner, a water machine, and a whiteboard. The layout and sizes of main objects in the office are shown in Fig. 1(b). The walls, floor and ceiling are made of concrete. Parts of the floor and ceiling are made of anti-static-electricity board. There are several windows on both sides of the wall.

B. Measurement System Setup

The channel sounder consists of a Keysight N5227A VNA, a series of standard gain horn antennas, a biconical antenna, an antenna positioner, cables, connectors, a tripod, and a laptop. The intermediate frequency (IF) filter bandwidth is set to 500 Hz to reduce the power level of the noise floor. Port 1 of the VNA sends the transmitted frequency sweeping signal and is connected to the Tx antenna, while Port 2 receives the fading signal and is connected to the Rx antenna. Thus, the S_{21} parameter is the channel transfer function between Tx and Rx, and the channel impulse response can be obtained by the inverse Fourier transform. The antenna locations are shown in Fig. 1(b). The coordinate of the Rx antenna is (1, 3, 1.45), and the coordinates of Tx antennas are (4, 2.2, 2.6), (3.2, 2.4, 2.6), (3.6, 3, 2.6), and (2, 5.2, 2.6). As a single horn antenna cannot cover the whole 10-40 GHz frequency bands, at the Tx side, four standard gain vertical polarized horn antennas working at 10–15, 15–22, 22–33, and 33–50 GHz bands are used to measure 11, 16, 28, and 38 GHz frequency bands, respectively. For each frequency band, the antenna gain is 10 dB with a half power beamwidth (HPBW) of 55° to cover a large space. The Rx antenna is a vertical polarized biconical antenna working at 3–40 GHz bands with gain of 3 dB. Its radiation pattern is omni-directional for the whole bands. During the measurement, the Tx antenna was aligned to the center of the Rx antenna array and placed on a tripod at four locations, while the Rx antenna was placed on an antenna positioner to shift positions to form a virtual antenna array. The measurements are conducted automatically with the environment being kept quasi-static. Before the measurement, a back-to-back calibration is conducted to remove the responses of the measurement system and the cables for each frequency band.

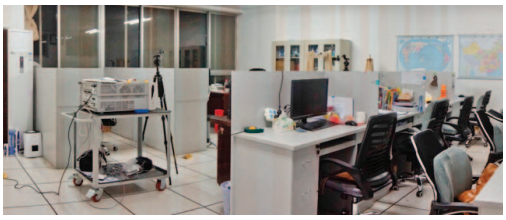

(a)

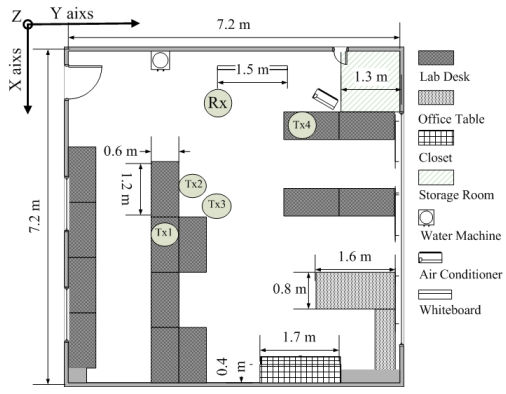

(b)

Fig. 1. (a) Photo of the environment and (b) Layout of the environment.

Rayleigh distance R is defined as $R = \frac{2D^2}{\lambda}$, where λ is the wavelength, and D in general can be taken as the maximum dimension of the antenna. For $N \times N$-element uniform rectangular array (URA) with a spacing step d, D is taken as $\sqrt{2}(N-1)d$. Then, the Rayleigh distance R is given as $4d^2(N-1)^2/\lambda$. When the distance between Tx and Rx antennas is smaller than Rayleigh distance, this propagation region is called the near field region or Fresnel region. If the distance is larger than that, this propagation region is called the far field region or Fraunhofer region.

At each frequency band and each Tx antenna location, the Rx antenna shifts positions in space to form a virtual antenna array with a spacing step less than half wavelength. The measurement system setup for the four bands is shown in Table I, while the antenna array configuration is shown in Table II. For 11 and 16 GHz lower bands, the signal bandwidth is 2 GHz and the delay resolution is 0.5 ns. For 28 and 38 GHz higher bands, the signal bandwidth is 4 GHz and the delay resolution is 0.25 ns. The frequency resolution for the four bands is 5 MHz. The spacing steps for the four bands are 12, 8, 4, and 3 mm, which are within half-wavelength and about 0.44, 0.43, 0.37, and 0.38, respectively, when normalized to the corresponding wavelengths. For the four bands, the calculated Rayleigh distances are within the Tx–Rx distances, which fulfil the far field and plane wavefront assumptions.

III. Measurement Data Processing Methods

A. The SAGE Algorithm

For VNA-based channel measurements, due to the quasi-static nature of the environment and relatively long measurement time, a large number of snapshots are not available. In reality, there is only a single snapshot. Thus, conventional subspace based high resolution algorithms like multiple signal classification (MUSIC) and estimation of signal parameters via rotational invariance technique (ESPRIT) can not be used, because these algorithms rely on an estimation of the noise covariance matrix which is rank deficient in the single-snapshot scenario. The maximum likelihood (ML) based SAGE algorithm [19] is applied to the data post-processing instead.

In the SAGE algorithm, the number of MPCs L is usually predefined large enough to capture all the significant paths. Some values for the numbers of MPCs have been investigated. We found that when the number of MPCs equals 100, a good trade-off between accuracy and computational complexity can be achieved. The outputs of the SAGE algorithm are the parameter sets $\mathbf{\Theta}_l = [\alpha_l, \tau_l, \phi_l, \theta_l], l = 1, ..., L$, where α_l, τ_l, ϕ_l, and θ_l denote the complex amplitude, delay, azimuth angle, and elevation angle for the lth MPC. These spatial-temporal MPC parameters are used to obtain some important propagation channel characteristics.

B. Propagation Channel Characteristics

1) APDP and RMS DS: The channel transfer function $\mathbf{H} \in C^{N^2 \times K}$ can be obtained by synthesizing the estimated MPCs

$$\mathbf{H}(n,k) = \sum_{l=1}^{L} \alpha_l \mathrm{exp}(\mathrm{j}2\pi\lambda^{-1} \langle e(\mathbf{\Omega}_l), r_n \rangle) \mathrm{exp}(-\mathrm{j}2\pi f_k \tau_l) \quad (1)$$

$$\begin{aligned} \langle e(\mathbf{\Omega}_l), r_n \rangle =& [x_n, y_n, z_n] \\ & \times [\cos(\phi_l)\sin(\theta_l), \sin(\phi_l)\sin(\theta_l), \cos(\theta_l)]^{\mathrm{T}} \end{aligned} \quad (2)$$

where N^2 is the number of array elements, K is the sweeping points, f_k denotes the kth frequency point, and x_n, y_n, and z_n denote the coordinates of the nth antenna array element.

The channel impulse response can be obtained by the inverse Fourier transform. For the measurement and estimated data, the APDP is obtained by averaging over the array elements

$$APDP = \frac{1}{N^2} \sum_{n=1}^{N^2} \left| IFFT(H(n, 1:K)) \right|^2. \quad (3)$$

The RMS DS is calculated as

$$DS = \sqrt{\frac{\sum_1^L |\alpha_l|^2 \tau_l^2}{\sum_1^L |\alpha_l|^2} - (\frac{\sum_1^L |\alpha_l|^2 \tau_l}{\sum_1^L |\alpha_l|^2})^2}. \quad (4)$$

2) PAP, PEP, and RMS AS: The PAP and PEP can be obtained as

$$PAP = \sum_{l=1}^{L} |\alpha_l|^2 \delta(\phi - \phi_l) \quad (5)$$

$$PEP = \sum_{l=1}^{L} |\alpha_l|^2 \delta(\theta - \theta_l) \quad (6)$$

where $\delta()$ is the Dirac delta function.

Note that the power of estimated MPCs with the same azimuth or elevation angles are summed up to get unique values.

Similar to the calculation of RMS DS, the RMS AS is calculated as

$$AS = \sqrt{\frac{\sum_1^L |\alpha_l|^2 \psi_l^2}{\sum_1^L |\alpha_l|^2} - (\frac{\sum_1^L |\alpha_l|^2 \psi_l}{\sum_1^L |\alpha_l|^2})^2} \quad (7)$$

where ψ_l denotes the azimuth angle ϕ_l or elevation angle θ_l.

IV. Results and Analysis

There are some important channel propagation characteristics for channel modeling, among which are the APDP, PAP, PEP, RMS DS, and azimuth and elevation AS. At this section, these properties will be compared and analyzed for the four mmWave frequency bands at the four Tx locations.

A. APDP

The measured and estimated APDPs are compared for the four frequency bands at Tx1 location, as shown in Fig. 2. For each frequency band, the estimated results match well with the measured data. Most of the MPCs are extracted accurately. A strong LOS path is seen with the same delay but different power gains. When the frequency increases, the attenuation tends to be larger. The reflected and scattered MPCs also show some different characteristics. The maximum excess delay is within 80 ns. Apart from the LOS path, an average of five clusters of MPCs are seen for the four bands.

B. PAP and PEP

The PAP and PEP are related with the measurement environment. Fig. 3 shows the PAPs at the four Tx locations for the four frequency bands. The azimuth angles show almost the same properties for different frequency bands at the same Tx location. An average of five clusters in azimuth domain are seen. The PAPs validation is shown in Fig. 4. For each Tx location, the LOS direction is pointed to the Rx antenna, while other reflection MPCs can be related to scatterers in the environment according to the delay and angle information. The PEPs at Tx1 are shown in Fig. 5. Because the Tx and Rx antenna height differences are the same for the four Tx locations, the elevation angles also show similar properties. The azimuth and elevation angles are sparse in space, and the beams are very narrow.

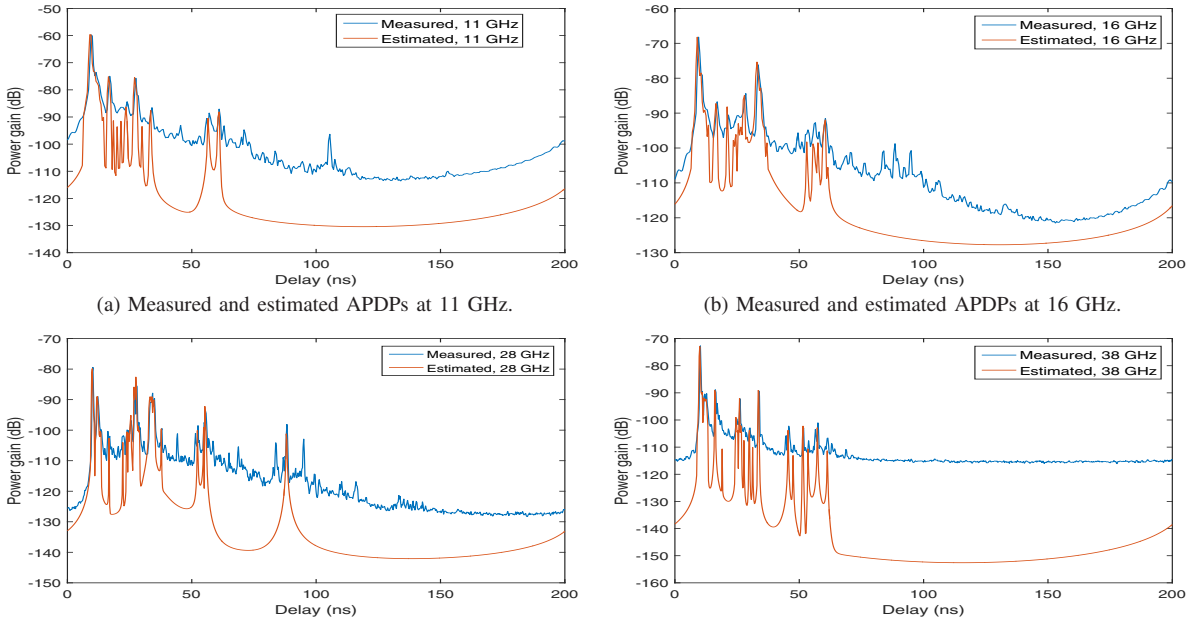

(a) Measured and estimated APDPs at 11 GHz.

(b) Measured and estimated APDPs at 16 GHz.

(c) Measured and estimated APDPs at 28 GHz.

(d) Measured and estimated APDPs at 38 GHz.

Fig. 2. (a) Measured and estimated APDPs at 11 GHz; (b) Measured and estimated APDPs at 16 GHz; (c) Measured and estimated APDPs at 28 GHz; (d) Measured and estimated APDPs at 38 GHz.

TABLE I
MEASUREMENT SYSTEM SETUP.

Center frequency (GHz)	11	16	28	38
Wavelength (mm)	27	19	11	8
Bandwidth (GHz)	2	2	4	4
Delay resolution (ns)	0.5	0.5	0.25	0.25
Output power (dBm)	15	15	13	8
Sweeping points	401	401	801	801

TABLE II
ANTENNA ARRAY CONFIGURATION.

Center frequency (GHz)	11	16	28	38
Spacing step (mm)	12	8	4	3
Array elements	10×10	15×15	15×15	20×20
Rayleigh distance (m)	1.7	2.7	1.2	1.6

TABLE III
AVERAGE RMS DS AND AS FOR THE FOUR BANDS.

Center frequency (GHz)	11	16	28	38
DS (ns)	9.3	10.3	10.6	8.2
Azimuth AS (°)	68.6	70.3	64.2	57.0
Elevation AS (°)	27.4	25.6	24.2	25.3

C. RMS DS and AS

Table III shows the RMS DS and AS for the four bands averaging over the four Tx locations. Generally, the RMS DS, azimuth AS, and elevation AS show similar values for different bands, which indicate that there are no large differences for the characterization of 10–40 GHz bands.

V. CONCLUSIONS

In this paper, we have conducted channel measurements at 11, 16, 28, and 38 GHz frequency bands in an indoor office environment. The measurement data have been processed with the SAGE algorithm, and some important channel propagation characteristics like APDP, PAP, PEP, RMS DS, and azimuth and elevation AS have been obtained and compared for the four frequency bands. The propagation characteristics of the four bands show similar properties, which indicate that the derivation of a unified mmWave channel model framework for 10–40 GHz is possible.

ACKNOWLEDGMENT

The authors would like to acknowledge the support from the EU H2020 ITN 5G Wireless project (Grant No. 641985), EU FP7 QUICK project (Grant No. PIRSES-GA-2013-612652), EPSRC TOUCAN project (Grant No. EP/L020009/1), National Science and Technology Major Project (Grant No. 2014ZX03003012-001), 863 Project in 5G (Grant No. 2014AA01A707), and Natural Science Foundation of China (Grant No. 61210002, 61371110).

REFERENCES

[1] C.-X. Wang, F. Haider, X. Gao, X.-H. You, Y. Yang, D. Yuan, H. Aggoune, H. Haas, S. Fletcher, and E. Hepsaydir, "Cellular architecture and key technologies for 5G wireless communication networks," *IEEE Commun. Mag.*, vol. 52, no. 2, pp. 122–130, Feb. 2014.

[2] T. S. Rappaport, S. Sun, R. Mayzus, H. Zhao, Y. Azar, K. Wang, G. N. Wong, J. K. Schulz, M. Samimi, and F. Gutierrez, "Millimeter wave mobile communications for 5G cellular: It will work!" *IEEE Access*, vol. 1, pp. 335–349, May 2013.

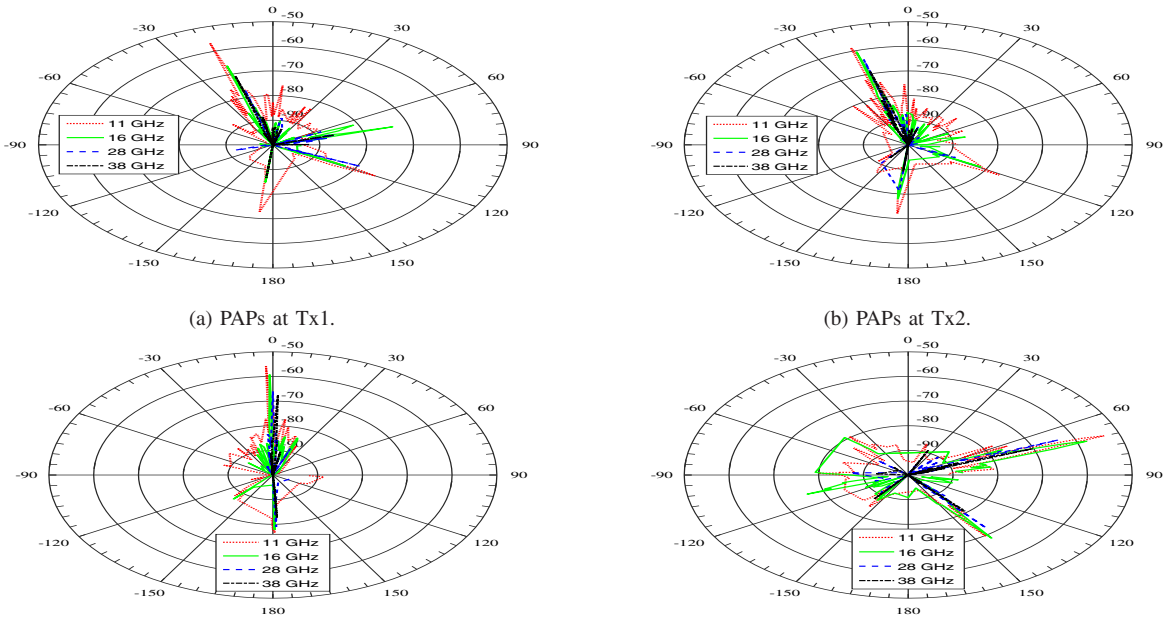

(a) PAPs at Tx1.

(b) PAPs at Tx2.

(c) PAPs at Tx3.

(d) PAPs at Tx4.

Fig. 3. (a) PAPs at Tx1; (b) PAPs at Tx2; (c) PAPs at Tx3; (d) PAPs at Tx4.

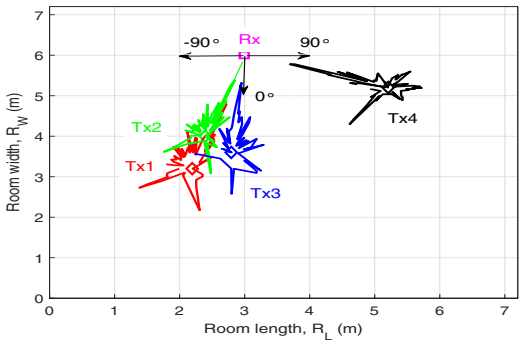

Fig. 4. PAPs validation for the measurement environment.

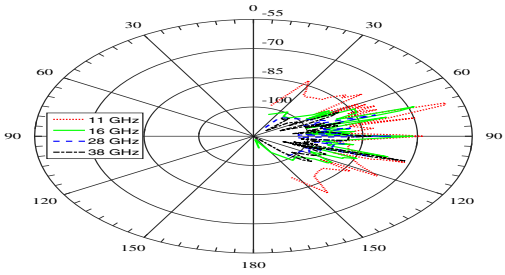

Fig. 5. PEPs for Tx1.

[3] METIS Website, [Online]. Available: https://www.metis2020.com/

[4] MIWEBA Website, [Online]. Available: http://www.miweba.eu/#Start

[5] mmMAGIC Website, [Online]. Available: https://5g-mmmagic.eu/

[6] 5GCM Website, [Online]. Available: http://www.5gworkshops.com/5GCM.html

[7] 3GPP Website, [Online]. Available: http://www.3gpp.org/DynaReport/38900.htm

[8] NYU Wireless Website, [Online]. Available: http://wireless.engineering.nyu.edu/nyusim/

[9] M. Kim, J. Takada, Y. Chang, J. Shen, and Y. Oda, "Large scale characteristics of urban cellular wideband channels at 11 GHz," in *Proc. EuCAP'15*, Lisbon, Portugal, Apr. 2015, pp. 1–4.

[10] X. Zhou, Z. Zhong, B. Zhang, R. He, K. Guan, Q. Wang, and D. Matolak, "Experimental characterization and correlation analysis of indoor channels at 15 GHz," *Int. J. Antennas Propag.*, Article ID 601835, 2015.

[11] X. Yin, C. Ling, and M.-D. Kim, "Experimental multipath cluster characteristics of 28 GHz propagation channel in office environments," *IEEE Access*, vol. 3, pp. 3138–3150, 2015.

[12] S. Hur, Y.-J. Cho, T. Kim, J. Park, A. F. Molisch, K. Haneda, and M. Peter, "Wideband spatial channel model in an urban cellular environments at 28 GHz," in *Proc. EuCAP'15*, Lisbon, Portugal, Apr. 2015, pp. 1–5.

[13] I. Rodriguez, H. C. Nguyen, T. B. Sorensen, J. Elling, J. A. Holm, P. Mogensen, P. Mogensen, and B. Vejlgaard, "Analysis of 38 GHz mmWave propagation characteristics of urban scenarios," in *Proc. European Wireless*, Budapest, Hungary, May 2015, pp. 1–8.

[14] S. Wyne, K. Haneda, S. Ranvier, F. Tufvesson, and A. F. Molisch, "Beamforming effects on measured mm-Wave channel characteristics," *IEEE Trans. Wireless Commun.*, vol. 10, no. 10, pp. 3553–3559, Nov. 2011.

[15] T. S. Rappaport, E. Ben-Dor, J. N. Murdock, and Y. Qiao, "38 GHz and 60 GHz angle-dependent propagation for cellular & peer-to-peer wireless communications," in *Proc. IEEE ICC'12*, Ottawa, Canada, Jun. 2012, pp.4568–4573.

[16] Y. Azar, G. N. Wong, K. Wang, R. Mayzus, J. K. Schulz, H. Zhao, F. Gutierrez, D. Hwang, and T. S. Rappaport, "28 GHz propagation measurements for outdoor cellular communications using steerable beam antennas in New York city," in *Proc. IEEE ICC'13*, Budapest, Hungary, Jun. 2013, pp.5143–5147.

[17] G. R. MacCartney and T. S. Rappaport, "73 GHz millimeter wave propagation measurements for outdoor urban mobile and backhaul communications in New York city," in *Proc. IEEE ICC'14*, Jun. 2014, Sydney, NSW, pp. 4862–4867.

[18] X. Wu, C.-X. Wang, J. Sun, J. Huang, R. Feng, Y. Yang, and X. Ge, "60 GHz millimeter-wave channel measurements and modeling for indoor office environments," *IEEE Trans. Antennas Propag.*, 2017, in press.

[19] B. H. Fleury, M. Tschudin, R. Heddergott, D. Dahlhaus, and K. I. Pedersen, "Channel parameter estimation in mobile radio environments using the SAGE algorithm," *IEEE J. Sel. Areas Commun.*, vol. 17, no. 3, pp. 434–450, Mar. 1999.